Scientific Reports

https://doi.org/10.1038/s41598-026-60630-7

Article in Press

Comparative essential oil profiling and pathway mapping of *Juniperus communis* and *Juniperus sabina*

Received: 5 February 2026

Accepted: 29 June 2026

Published online: 10 July 2026

Cite this article as: Mohebodini M., Ghanbari Moheb Seraj R. & Tariverdizadeh N. Comparative essential oil profiling and pathway mapping of *Juniperus communis* and *Juniperus sabina*. *Sci Rep* (2026). https://doi.org/10.1038/s41598-026-60630-7

Mehdi Mohebodini, Rahele Ghanbari Moheb Seraj & Neda Tariverdizadeh

Comparative essential oil profiling and pathway mapping of *Juniperus communis* and *Juniperus sabina*

Mehdi Mohebodini[1*], Rahele Ghanbari Moheb Seraj[1], Neda Tariverdizadeh[1]

[1]Department of Horticultural Sciences, Faculty of Agriculture and Natural Resources, University of Mohaghegh Ardabili, Ardabil, Iran

* Corresponding authors: e-mail: mohebodini@uma.ac.ir

Abstract

This study provides a comparative characterization of the essential oil profiles and database-supported pathway mapping of *Juniperus communis* and *Juniperus sabina* collected from the Salouk region of North Khorasan, Iran. Essential oils were extracted by hydrodistillation, analyzed using GC–MS, statistically compared between species, and interpreted through multivariate analysis and pathway mapping based on KEGG, UniProt, MetaCyc, and supporting literature. Essential oil yield was markedly higher in *J. sabina* than in *J. communis* (1.70 and 0.54 g per 100 g dried material, respectively). A total of 63 volatile compounds were identified, with significant interspecific differences for most evaluated metabolites. *J. communis* was mainly characterized by higher relative abundances of *trans*-pinene (15.00%), *α*-phellandrene (14.97%), *α*-pinene (11.28%), terpinolene (6.66%), and *trans*-sabinene acetate (5.02%). In contrast, *J. sabina* showed higher levels of sabinene (12.78%), camphene (10.12%), terpinolene (8.04%), *α*-terpinene (6.78%), 3-octanol (4.75%), *δ*-terpinyl acetate (3.83%), and linalool (3.38%). PCA revealed a clear separation between the two species, with the first two dimensions explaining 99.94% of the total variance, indicating that species differentiation was driven by coordinated changes across multiple volatile constituents. Pathway mapping assigned 49 of the 63 detected compounds, approximately 77.78%, to GPP-related routes, highlighting the predominance of monoterpene-derived compounds in both essential oils. Additional metabolites were associated with PEP-, shikimate/phenylalanine-, acetyl-CoA-, valine-, and FPP-related routes, providing a broader biochemical organization of the detected compounds. Overall, the results demonstrate strong chemical differentiation between *J. communis* and *J. sabina* and identify dominant and species-associated volatile metabolites that may serve as candidate markers for phytochemical characterization, essential oil quality assessment, chemotaxonomic comparison, and future bioactivity-focused studies.

Keywords

Juniperus communis; *Juniperus sabina*; Essential oil; GC–MS; Monoterpenes; Geranyl diphosphate; Pathway mapping; Principal component analysis

Introduction

Understanding the intricate metabolic networks underlying the biosynthesis of plant natural products is fundamental for exploring the chemical complexity of medicinal species such as *Juniperus communis* and *Juniperus sabina*. The genus Juniperus (family Cupressaceae), comprising approximately 70–80 species, is recognized as a rich source of structurally diverse secondary metabolites—including terpenoids, flavonoids, lignans, and phenolic acids—which contribute to its pharmacological potential and ecological functions (Pan et al., 2024) and have been historically and contemporarily used in traditional medicine (Tavares and Seca, 2018; Mohammad et al., 2025).

Plant secondary metabolites arise from the dynamic interplay between primary metabolism and specialized biosynthetic pathways. Central metabolites such as phosphoenolpyruvate (PEP) act as key junctions, linking core carbon flux with downstream pathways that generate both primary building blocks and complex bioactive compounds (Hu et al., 2025). PEP, produced through glycolytic processes, serves not only as an intermediate in energy metabolism but also as a substrate for essential anabolic pathways, including the shikimate and methylerythritol phosphate (MEP) pathways, which collectively support the biosynthesis of aromatic amino acids and isoprenoid-derived metabolites (Di, 2022; Mohammadi et al., 2025). In plastids, PEP together with erythrose-4-phosphate drives the shikimate pathway, ultimately leading to the formation of chorismate—a precursor to aromatic amino acids such as phenylalanine, a gateway molecule for phenylpropanoid biosynthesis (Yokoyama et al., 2021).

The integration of these central metabolic hubs with specialized biosynthetic systems allows plants to modulate their chemical output in response to developmental cues and environmental pressures (Pott et al., 2019; Ghanbari Moheb Seraj et al., 2025a, b). In juniper species, this complexity is reflected in the diversity of essential oil constituents and other secondary metabolites, which have been characterized across plant organs and seasonal conditions using GC-MS and NMR-based metabolomic approaches (Butkienė et al., 2015; Shahbazi et al., 2022). However, most previous studies have primarily focused on reporting compound identities, relative abundances, and chemotypic variation, whereas fewer studies have attempted to connect GC–MS-detected volatile constituents with known biosynthetic pathways in a

comparative and database-supported framework. Therefore, a clear research gap remains in the cautious integration of comparative essential oil profiling with putative biosynthetic pathway interpretation, particularly for medicinally relevant species such as *J. communis* and *J. sabina*.

The selection of *J. communis* and *J. sabina* was based on their taxonomic relatedness, aromatic and medicinal relevance, and reported differences in volatile chemical composition. Because both species belong to the same genus but may differ in the relative accumulation of monoterpenes, oxygenated terpenes, esters, and sesquiterpenes, their comparison provides a useful basis for evaluating species-associated chemical differentiation.

We hypothesized that *J. communis* and *J. sabina* differ in their essential oil composition and that these differences can be interpreted, in a database-supported manner, in relation to known biosynthetic pathways associated with terpenoid, phenylpropanoid, fatty acid-derived, and amino acid-derived volatile metabolites. Accordingly, the present study integrates GC–MS-based essential oil profiling, comparative metabolite assessment, and database-supported biosynthetic pathway interpretation. Biosynthetic pathways were inferred through data mining, published literature, and authoritative databases such as KEGG and UniProt. However, the inferred pathways and associated enzymes are considered putative and should not be interpreted as direct evidence of pathway activity, metabolic flux, or enzyme-level validation in these species.

The main objectives of this study were to: (i) characterize and compare the essential oil profiles of *J. communis* and *J. sabina* using GC–MS; (ii) identify shared and species-associated volatile constituents; and (iii) interpret the detected metabolites within a database-supported framework of putative biosynthetic pathways, including PEP-, shikimate/phenylalanine-, acetyl-CoA-, valine-, GPP-, and FPP-associated pathways. The novelty of this study lies not in experimentally validating biosynthetic enzymes or pathway activity, but in combining comparative GC–MS-based volatile profiling with cautious, database-guided biosynthetic mapping for these two *Juniperus* species. This approach provides a preliminary pathway-level framework for organizing the detected metabolites and identifying candidate compounds and putative pathways that may guide future molecular, enzymatic, ecological, and bioactivity-focused investigations.

Materials and Methods

Plant Material Collection

The plant material for this study was collected from two species, *J. communis* and *J. sabina*, in the Salouk region, south of Bojnord, North Khorasan, Iran, in 2023. For each species, three individual trees were selected, and from each tree, ten green shoots of similar size were sampled from different parts. The samples from each replicate were subsequently pooled, placed in separate bags, and transported to the laboratory. Collections were performed at elevations above 2,000 meters above sea level.

The collection sites are located within the geographic coordinates 37°15' N to 37°07' N latitude and 57°17' E to 57°03' E longitude. The region has a semi-arid climate with hot, dry summers and cold winters. Maximum temperatures reach 22.82 °C, while minimum temperatures range from –5 °C to 5 °C. Annual precipitation is approximately 200–400 mm, with relative humidity varying between 32.07% and 78.25%. All plant specimens were identified and verified by Dr. Farzaneh Khajoei Nasab, a botanist at Shahid Beheshti University. Herbarium specimens were registered at the Research and Education Center for Agriculture and Natural Resources of North Khorasan Province under the following reference numbers: *J. communis* (Khsh.CU/*J. communis* 101) and *J. sabina* (Khsh.CU/*J. sabina* 103). All necessary permissions for sample collection were obtained from the relevant authorities, in accordance with national and international guidelines. The collected samples were processed and stored under suitable conditions to ensure sample integrity for subsequent analyses.

Soil Sampling and Analysis

Soil samples were collected from beneath the canopy of *J. communis* and *J. sabina* at a depth of 30 cm from three points along a 100-meter transect in each habitat. The samples were air-dried, ground using a mortar, and sieved through a 2 mm mesh to ensure uniformity. Key physicochemical properties of the soil, including pH, electrical conductivity (EC), soil saturation percentage (SP), organic carbon content (O.C.), nitrogen (N), phosphorus (P), potassium (K), and various micronutrients, were analyzed to provide environmental background information for the sampling sites.

Essential Oil Extraction

The collected samples of *J. communis* and *J. sabina* were air-dried and ground. Essential oils (EOs) were extracted using a Clevenger apparatus via hydrodistillation for 2.5 hours for each sample. The extracted oils were dehydrated with sodium sulfate, and the essential oil yield for each sample was determined by weighing the dehydrated oil. The yield was expressed as

grams of essential oil per 100 g of dried plant material. Oils were stored in dark glass vials at 4°C and protected from light to preserve their composition until further analysis (Spengler et al., 2022).

GC–MS Analysis of Essential Oils

GC–MS analysis was performed to characterize the chemical constituents of the extracted essential oils. Samples were analyzed using a gas chromatograph-mass spectrometer equipped with an Rtx-5MS fused-silica capillary column (30 m length, 0.25 mm internal diameter, 0.25 µm film thickness). The injection volume was set at 1 µL, and a split ratio of 1:15 was applied to ensure optimal peak resolution and detector response, as commonly reported for volatile plant oils. Helium was used as the carrier gas at a constant flow rate of 1.0 mL/min, and the injector and transfer line temperatures were maintained at 250 °C and 280 °C, respectively. The oven temperature program began at 45 °C (held for 2 min), increased to 250 °C at a rate of 5 °C/min, and was held at the final temperature for 5 min. Mass spectra were acquired in full scan mode over the mass range of 40–500 m/z, using electron impact (EI) ionization at 70 eV, with the ion source temperature at 200 °C. Compound identification was achieved by comparing mass spectra and experimental retention indices (Kovats index, KI) with reference spectra from the NIST and Wiley mass spectral libraries and published literature, and by using a homologous series of n-alkanes (C8–C28) to calculate KI values for further confirmation of compound identity. The similarity threshold for library matching was set at ≥80% to ensure reliable identification (Ouakouak et al. 2019; El-Kased et al. 2022). Quantification of all identified compounds was performed based on relative peak area percentages, representing the proportion of each compound in the total chromatographic profile.

Statistical Analysis and Graphical Representation

Statistical analyses were performed using R software version 4.5.0 (R Core Team, 2025) in the RStudio graphical user interface version 2025.05.0 (Posit Team, 2025). For each identified compound, relative GC–MS peak area percentages were calculated from three biological replicates. Differences in metabolite relative abundance between *J. communis* and *J. sabina* were evaluated using one-way analysis of variance (ANOVA), with species considered as the fixed factor. Statistical significance was considered at $P < 0.05$ and $P < 0.01$.

The heatmap of metabolite relative abundance was generated in R using the ggplot2 package (Wickham, 2016). The relative GC–MS peak area percentages of the identified metabolites were used as input values, and the heatmap was drawn using tile-based visualization. No clustering, scaling, or additional normalization was applied; therefore, no clustering algorithm or distance metric was used. The color gradient represents the original relative abundance values of each metabolite in *J. communis* and *J. sabina*.

Principal component analysis (PCA) was performed to evaluate the multivariate variation in GC–MS metabolite profiles between *J. communis* and *J. sabina*. The analysis was conducted in R software using the RStudio graphical user interface. The input data consisted of relative GC–MS peak area percentages of 63 detected metabolites across six samples, including three biological replicates for each species. Prior to PCA, the data matrix was arranged with samples as rows and metabolites as variables. The dataset was mean-centered and scaled to unit variance before analysis to minimize the influence of differences in metabolite abundance ranges. PCA was performed using the PCA function from the *FactoMineR* package, and graphical visualization of the PCA biplot was generated using the *factoextra* and *ggplot2* packages. In the biplot, sample scores were displayed together with metabolite vectors to visualize the association of metabolites with the first two principal components.

Database Mining and Text Mining

Following GC–MS-based metabolite profiling, each identified compound was systematically examined to determine its possible biosynthetic origin and putative pathway association. The database-mining workflow was conducted using KEGG release 116.0 (Kanehisa et al., 2025; Kanehisa, 2019; Kanehisa and Goto, 2000), UniProt release 2025_04 (UniProt Consortium, 2018), and MetaCyc version 29.1, (Caspi et al. 2020) all accessed in October 2025. First, the compound names listed in Table 1 were used as the primary search terms and were searched in KEGG, UniProt, and MetaCyc. When available, compound synonyms were also checked to improve database retrieval. If sufficient information for a metabolite was not found in these databases, the same compound name was searched in relevant literature sources, including scientific articles and books, to obtain information on its reported biosynthetic origin, related precursors, associated reactions, and possible pathway connections.

The main inclusion criterion for pathway mapping was the detection of the compound in the GC–MS profile of the present study. Therefore, only

metabolites identified in this study were placed in the pathway diagrams. Upstream precursors and intermediate compounds were included only when they were necessary to show the biosynthetic pathway leading to the detected metabolites. Pathways were selected when at least one identified metabolite, or a known precursor, product, or reaction related to that metabolite, was reported in KEGG, UniProt, MetaCyc, or supporting literature. Compounds for which no reliable pathway-related information was found were not assigned to a specific biosynthetic pathway.

The enzymes associated with each pathway were assigned based on KEGG, UniProt, and MetaCyc annotations. When direct database information was incomplete or unavailable, enzyme assignment was supported by published literature describing similar reactions or related biosynthetic pathways. Since enzyme activity was not experimentally measured in the present study, the enzymes shown in the pathway diagrams were used only to indicate reported reactions associated with the proposed biosynthetic pathways. The collected information was then used to reconstruct and illustrate the putative biosynthetic pathways of the identified metabolites by referring to KEGG pathway maps, MetaCyc pathway information, UniProt annotations, and literature-supported biochemical relationships.

The pathway diagrams were manually designed using Microsoft Word. The colored boxes representing the detected metabolites were prepared using a graded color scale in Microsoft Excel, based on the relative GC–MS peak area percentages of each compound in *J. communis* and *J. sabina.* This color coding was used only to visualize relative abundance differences between the two species within the proposed pathway diagrams. Finally, the reconstructed pathways and metabolite profiles were compared to identify major pathway-associated metabolites, species-specific compounds, and putative biosynthetic pathways related to the observed chemical differentiation between *J. communis* and *J. sabina*.

Results

Physicochemical Soil Properties

The physicochemical properties of the soil were analyzed before the experiment. The soil pH was 7.7, indicating a slightly alkaline reaction, which was above the desired range of 6.5–7.0. Electrical conductivity (EC) was 1.3 mS/cm, which was below the critical threshold of 3 mS/cm, indicating low soil salinity. The soil saturation percentage (SP) was 41%, slightly higher than the typical regional range of 35–40%. Organic carbon (O.C.) content was 2%,

which was at the upper limit or slightly above the recommended range of 1.5–2.0%. Total nitrogen content was 0.34%, exceeding the normal range of 0.1–0.2%. Available phosphorus (Pav) was 96.2 ppm, which was considerably higher than the standard range of 30–35 ppm, while available potassium (Kav) was within the expected range. Based on the particle-size distribution of 60% sand, 36% silt, and 4% clay, the soil texture was classified as sandy loam. The concentrations of micronutrients, including Fe, Cu, Mn, B, and Zn, were within the normal range for the region.

ANOVA of metabolite variation between Juniperus species

The analysis of variance (ANOVA) revealed significant differences between *J. communis* and *J. sabina* for the majority of the evaluated metabolites ($P < 0.01$). The species effect was highly significant for key terpenoid compounds including *α*-pinene, camphene, *trans*-pinene, sabinene, *α*-phellandrene, *α*-terpinene, and 3-octanol, indicating substantial metabolic divergence between the two Juniperus species. The relatively low standard deviations among biological replicates suggest acceptable experimental consistency and limited within-species variability in the relative abundance of most evaluated metabolites. The total variation observed in metabolite accumulation was therefore primarily associated with species-dependent biochemical differences rather than experimental variability. Among the analyzed compounds, *α*-phellandrene, *trans*-pinene, *α*-pinene, and camphene exhibited the highest mean square values, highlighting their important contribution to the metabolic differentiation between the two species.

Table 1. Comparative chemical composition of essential oils from *Juniperus communis* and *Juniperus sabina* based on GC–MS analysis. The table presents the identified metabolites, chemical classes, retention index/Kovats index values (RI/KI), relative GC–MS peak area percentages (%) in each species, occurrence pattern, and statistical significance. Values are expressed as mean ± standard deviation (SD) of relative peak area percentages based on three biological replicates. Statistical differences between *J. communis* and *J. sabina* were evaluated using one-way ANOVA. 0.00 ± 0.00 indicates that the compound was not detected under the analytical conditions used. ns, not significant; $P < 0.05$; ** $P < 0.01$.

Table 1. Comparative chemical composition of essential oils from *Juniperus communis* and *Juniperus sabina* based on GC–MS analysis. The table presents the identified metabolites, chemical classes, retention index/Kovats index values (RI/KI), relative GC–MS peak area percentages (%) in each species, occurrence pattern, and statistical significance. Values are expressed as mean ± standard deviation (SD) of relative peak area percentages based on three biological replicates. Statistical differences between *J. communis* and *J. sabina* were evaluated using one-way ANOVA. 0.00 ± 0.00 indicates that the compound was not detected under the analytical conditions used. ns, not significant; $P < 0.05$; ** $P < 0.01$.

Compound	Chemical class	RI/KI	*J. communis* (%)	*J. sabina* (%)	Occurrence	p-value	Sig.
α-Pinene	Monoterpene hydrocarbon	939	11.28 ± 0.45	0.00 ± 0.00	*J. communis* only	1.698E-06	**
α-Fenchene	Monoterpene hydrocarbon	952	1.97 ± 0.08	0.00 ± 0.00	*J. communis* only	1.718E-06	**
Camphene	Monoterpene hydrocarbon	954	0.00 ± 0.00	10.12 ± 0.41	*J. sabina* only	1.704E-06	**
Hexanoic acid	Fatty acid	973	0.00 ± 0.00	0.75 ± 0.03	*J. sabina* only	1.701E-06	**
trans-Pinene	Monoterpene hydrocarbon	978	15.00 ± 0.60	0.00 ± 0.00	*J. communis* only	1.701E-06	**
Sabinene	Monoterpene hydrocarbon	975	4.44 ± 0.38	12.78 ± 0.83	Both species	1.170E-05	**
1-Octen-3-ol	Alcohol / oxygenated volatile	979	3.23 ± 0.13	0.00 ± 0.00	*J. communis* only	1.690E-06	**
β-Pinene	Monoterpene hydrocarbon	979	0.00 ± 0.00	2.82 ± 0.11	*J. sabina* only	1.713E-06	**
trans-Isolimonene	Monoterpene hydrocarbon	984	1.34 ± 0.06	1.96 ± 0.08	Both species	3.472E-04	**
cis-Pinene	Monoterpene hydrocarbon	979	0.00 ± 0.00	2.42 ± 0.10	*J. sabina* only	1.715E-06	**
3-Octanol	Alcohol / oxygenated volatile	984	0.00 ± 0.00	4.75 ± 0.19	*J. sabina* only	1.701E-06	**
Ethyl hexanoate	Ester	983	0.00 ± 0.00	1.11 ± 0.04	*J. sabina* only	1.640E-06	**
α-Phellandrene	Monoterpene hydrocarbon	1002	14.97 ± 0.42	0.72 ± 0.24	Both species	2.083E-06	**
p-Mentha-1(7),8-diene	Monoterpene hydrocarbon	1004	0.99 ± 0.03	0.73 ± 0.02	Both species	8.037E-04	**
Dihydroxy *cis*-linalool oxide	Oxygenated monoterpene	1008	0.00 ± 0.00	0.50 ± 0.02	*J. sabina* only	1.701E-06	**
δ-3-Carene	Monoterpene hydrocarbon	1011	2.40 ± 0.10	0.00 ± 0.00	*J. communis* only	1.701E-06	**
α-Terpinene	Monoterpene hydrocarbon	1017	0.98 ± 0.09	6.78 ± 0.19	Both species	3.294E-06	**
p-Cymene	Monoterpene hydrocarbon	1024	2.27 ± 0.11	3.34 ± 0.13	Both species	3.330E-04	**
Methyl heptanoate	Ester	1025	0.00 ± 0.00	1.93 ± 0.08	*J. sabina* only	1.683E-06	**
Limonene	Monoterpene hydrocarbon	1029	0.79 ± 0.03	0.00 ± 0.00	*J. communis* only	1.788E-06	**

1,8-Cineole	Oxygenated monoterpene	1031	0.00 ± 0.00	2.47 ± 0.10	*J. sabina* only	1.714E-06	**
(Z)-*β*-Ocimene	Monoterpene hydrocarbon	1037	0.00 ± 0.00	0.94 ± 0.04	*J. sabina* only	1.774E-06	**
Isobutyl angelate	Ester	1051	0.80 ± 0.03	1.52 ± 0.05	Both species	5.474E-05	**
Bergamal	Oxygenated monoterpene / aldehyde	1056	2.27 ± 0.09	0.00 ± 0.00	*J. communis* only	1.716E-06	**
γ-Terpinene	Monoterpene hydrocarbon	1059	1.07 ± 0.04	0.76 ± 0.01	Both species	5.125E-04	**
Artemisia ketone	Oxygenated monoterpene / ketone	1062	0.00 ± 0.00	0.51 ± 0.02	*J. sabina* only	1.571E-06	**
Terpinolene	Monoterpene hydrocarbon	1088	6.66 ± 0.23	8.04 ± 0.30	Both species	4.614E-03	**
Linalool	Oxygenated monoterpene / alcohol	1096	0.88 ± 0.03	3.38 ± 0.10	Both species	6.412E-06	**
trans-Sabinene hydrate	Oxygenated monoterpene	1098	0.00 ± 0.00	0.91 ± 0.04	*J. sabina* only	1.627E-06	**
cis-Thujone	Oxygenated monoterpene / ketone	1102	0.00 ± 0.00	0.50 ± 0.02	*J. sabina* only	1.701E-06	**
Isopentyl isovalerate	Ester	1103	0.67 ± 0.03	0.61 ± 0.03	Both species	4.516E-02	*
trans-Thujone	Oxygenated monoterpene / ketone	1114	0.73 ± 0.03	1.13 ± 0.04	Both species	2.056E-04	**
α-Campholenal	Oxygenated monoterpene / aldehyde	1126	0.00 ± 0.00	1.16 ± 0.05	*J. sabina* only	1.643E-06	**
Camphor	Oxygenated monoterpene / ketone	1146	0.00 ± 0.00	1.20 ± 0.05	*J. sabina* only	1.701E-06	**
Borneol	Oxygenated monoterpene / alcohol	1169	0.81 ± 0.04	1.07 ± 0.06	Both species	1.098E-03	**
α-Terpineol	Oxygenated monoterpene / alcohol	1188	1.04 ± 0.04	0.48 ± 0.03	Both species	3.016E-05	**
Verbenone	Oxygenated monoterpene / ketone	1205	0.65 ± 0.03	0.00 ± 0.00	*J. communis* only	1.701E-06	**
cis-Sabinene hydrate acetate	Oxygenated monoterpene ester	1221	0.00 ± 0.00	0.52 ± 0.02	*J. sabina* only	1.767E-06	**
Hexyl isovalerate	Ester	1244	1.21 ± 0.04	0.71 ± 0.02	Both species	9.898E-05	**
cis-Myrtanol	Oxygenated monoterpene / alcohol	1253	1.43 ± 0.06	0.00 ± 0.00	*J. communis* only	1.677E-06	**
trans-Sabinene acetate	Oxygenated monoterpene ester	1256	5.02 ± 0.15	1.10 ± 0.05	Both species	5.030E-06	**
trans-Myrtanol	Oxygenated monoterpene / alcohol	1261	1.32 ± 0.05	1.23 ± 0.04	Both species	9.693E-02	ns
Isopropyl phenylacetate	Aromatic ester / phenylpropanoid-related	1270	0.65 ± 0.03	0.00 ± 0.00	*J. communis* only	1.701E-06	**
α-Terpinene-7-al	Oxygenated monoterpene / aldehyde	1285	1.43 ± 0.04	1.38 ± 0.06	Both species	3.357E-01	ns
Bornyl acetate	Oxygenated monoterpene ester	1285	0.00 ± 0.00	2.55 ± 0.10	*J. sabina* only	1.701E-06	**
trans-Sabinyl acetate	Oxygenated monoterpene ester	1290	0.73 ± 0.03	0.89 ± 0.04	Both species	3.895E-03	**
γ-Terpinene-7-al	Oxygenated monoterpene / aldehyde	1291	0.67 ± 0.03	0.00 ± 0.00	*J. communis* only	1.752E-06	**

Methyl acetate	Ester	523	1.14 ± 0.03	1.65 ± 0.06	Both species	3.909E-04	**
Geranyl formate	Monoterpene ester	1298	1.93 ± 0.08	0.00 ± 0.00	*J. communis* only	1.683E-06	**
Terpinen-4-ol acetate	Oxygenated monoterpene ester	1299	0.00 ± 0.00	1.99 ± 0.08	*J. sabina* only	1.735E-06	**
δ-terpinyl acetate	Oxygenated monoterpene ester	1317	0.80 ± 0.01	3.83 ± 0.11	Both species	4.694E-06	**
Myrtenyl acetate	Oxygenated monoterpene ester	1326	1.08 ± 0.04	0.00 ± 0.00	*J. communis* only	1.669E-06	**
p-Mentha-1,4-dien-7-ol	Oxygenated monoterpene / alcohol	1327	0.83 ± 0.06	1.91 ± 0.06	Both species	2.279E-05	**
trans-Carvyl acetate	Oxygenated monoterpene ester	1342	0.00 ± 0.00	0.47 ± 0.02	*J. sabina* only	1.774E-06	**
Verbenol acetate	Oxygenated monoterpene ester	1292	0.00 ± 0.00	1.89 ± 0.08	*J. sabina* only	1.737E-06	**
Benzyl butanoate	Aromatic ester / phenylpropanoid-related	1346	1.41 ± 0.06	0.00 ± 0.00	*J. communis* only	1.653E-06	**
α-terpinyl acetate	Oxygenated monoterpene ester	1349	0.00 ± 0.00	2.85 ± 0.11	*J. sabina* only	1.701E-06	**
α-Cubebene	Sesquiterpene hydrocarbon	1351	1.70 ± 0.07	0.00 ± 0.00	*J. communis* only	1.701E-06	**
α-Copaene	Sesquiterpene hydrocarbon	1376	0.71 ± 0.03	0.00 ± 0.00	*J. communis* only	1.607E-06	**
Hexyl hexanoate	Ester	1383	0.83 ± 0.03	0.00 ± 0.00	*J. communis* only	1.660E-06	**
β-Bourbonene	Sesquiterpene hydrocarbon	1388	1.76 ± 0.07	0.00 ± 0.00	*J. communis* only	1.662E-06	**
β-Elemene	Sesquiterpene hydrocarbon	1390	1.02 ± 0.04	0.00 ± 0.00	*J. communis* only	1.734E-06	**
α-Cadinene	Sesquiterpene hydrocarbon	1538	0.00 ± 0.00	0.57 ± 0.02	*J. sabina* only	1.761E-06	**

Essential Oil Yield in Shoots

Essential oil yields from the shoots of *J. communis* and *J. sabina* were determined at 0.54 g and 1.7 g per 100 g of dried material, respectively, indicating a notably higher oil content in *J. sabina*. These data provide a quantitative basis for subsequent chemical characterization and comparative analyses between the two species.

Metabolite Profiling

The results revealed significant differences in metabolite percentages between the two species of *J. communis* and *J. sabina*, which could be linked to their distinct plant chemistry and biosynthetic pathways. *J. communis* exhibited higher percentages of key metabolites such as *α*-pinene (11.28%), *α*-phellandrene (14.97%), and *trans*-pinene (15%), suggesting the presence of specific biosynthetic pathways in this species. These compounds are primarily involved in terpene production and aromatic compounds. Additionally, *J. sabina* contained unique metabolites like *α*-campholenal, camphor, and Bornyl acetate, which were not found in *J. communis*.

In contrast, *J. sabina* showed higher percentages of metabolites such as camphene (10.12%), sabinene (12.78%), and *cis*-sabinene hydrate acetate (0.52%). These findings suggest distinct biosynthetic pathways and the presence of oxygenated terpenes like sabinene and camphene in this species. Furthermore, certain metabolites like terpinen-4-ol acetate (1.99%) and *cis*-sabinene hydrate acetate (0.52%) were only found in *J. sabina*, indicating unique chemical characteristics of this species. The observed differences in metabolite percentages and compound types may be attributed to genetic and ecological differences between the two species, which result in distinct metabolic and defensive strategies. These data emphasize the need for further investigation into biosynthetic pathways and the potential role of metabolites in environmental adaptation.

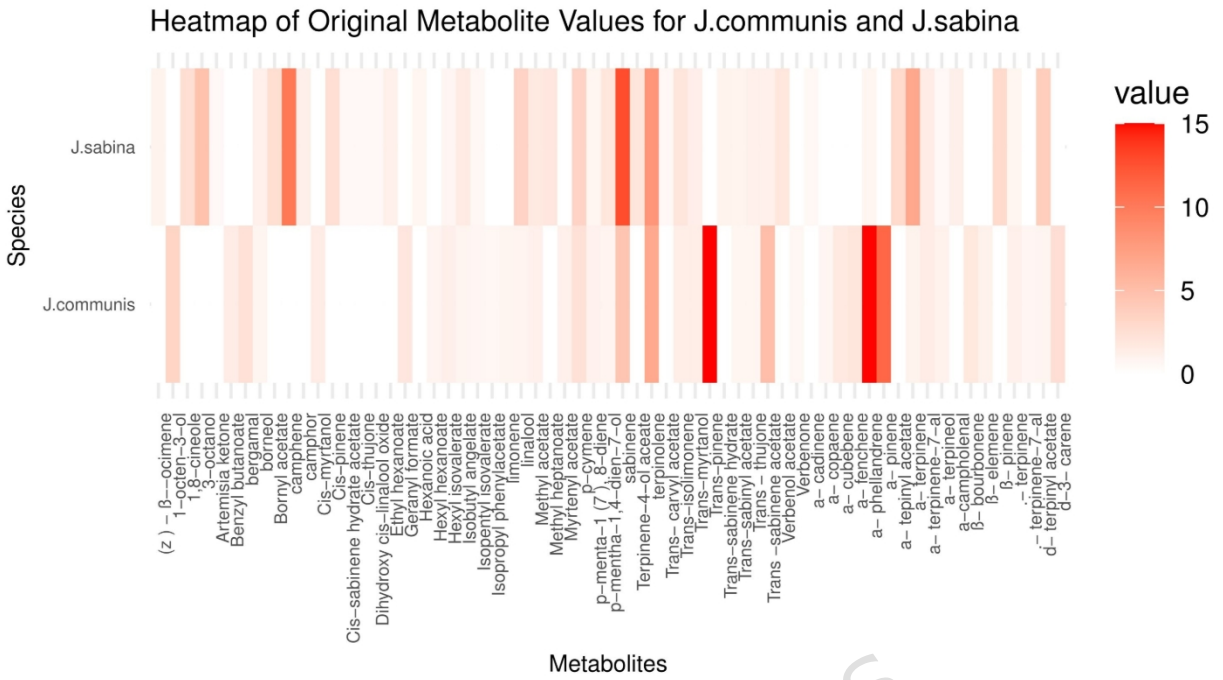

Figure 1. Heatmap of the relative abundance of identified metabolites in *Juniperus communis* and *Juniperus sabina*. Metabolite values are expressed as relative GC–MS peak area percentages (%), representing the proportion of each compound in the total chromatographic profile. Rows correspond to the two Juniperus species and columns represent the identified metabolites. The color gradient indicates variation in relative abundance, with lighter colors representing lower values and darker red colors representing higher values.

Biosynthesis pathways

The results obtained from the analysis of biosynthetic pathways in *J. communis* and *J. sabina* reveal significant differences in the relative abundance of pathway-associated metabolites between the two species. In this study, the key biosynthetic pathways associated with Phosphoenolpyruvic acid (PEP) in two species were examined and analyzed. PEP traverses two primary biosynthetic pathways: the shikimate pathway and the pyruvate pathway. In the shikimate pathway, PEP leads to the synthesis of phenylalanine, which serves as a critical precursor for the production of phenolic and antioxidant compounds. On the other hand, in the pyruvate pathway, various products, including valine and acetyl-CoA, are synthesized. Acetyl-CoA plays a central role in the biosynthesis of fatty acids, which are essential for cell membrane structure and energy storage in plants. Additionally, methanol is incorporated as a precursor in this pathway and is converted into methyl acetate by the enzyme alcohol acyltransferase. The amounts of methyl acetate produced in *J. sabina* and *J. communis* were 1.65% and 1.14%, respectively. Another pathway derived from PEP is the MEP

pathway, where IPP and DMAPP are sequentially synthesized. These compounds then proceed to generate GPP and FPP in subsequent reactions. The highlighted products in these pathways act as precursors for other biosynthetic pathways. In each of these pathways, various metabolites were identified, and their quantities were meticulously measured and analyzed, as detailed in the subsequent sections of the manuscript (Fig. 2).

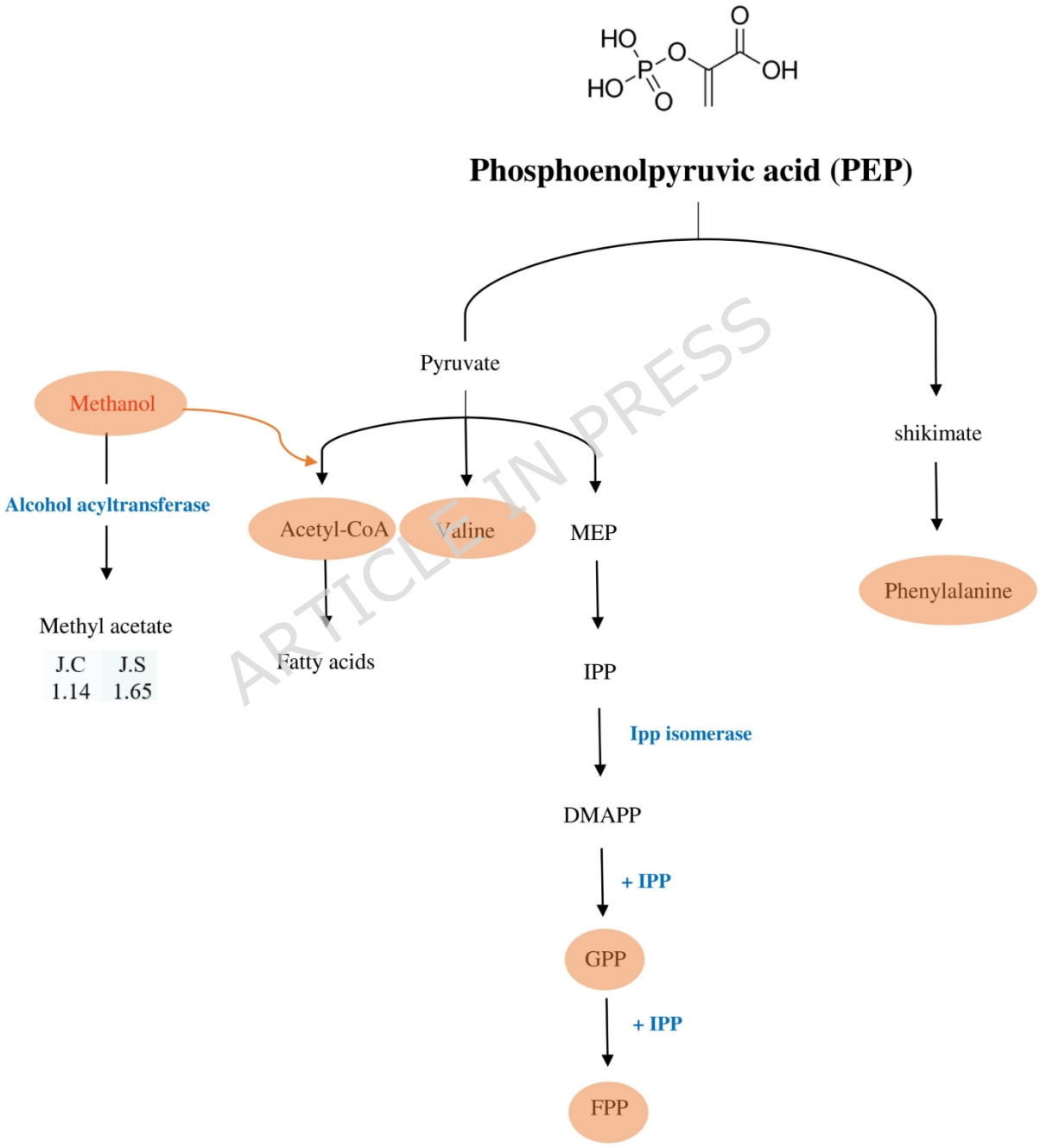

Figure 2. Schematic representation of putative biosynthetic pathways originating from phosphoenolpyruvic acid (PEP) in *Juniperus sabina* (JS) and *Juniperus communis* (JC). The highlighted compounds in orange represent selected upstream intermediates related to downstream biosynthetic pathways. The pathway illustrates the substrates, products, and reported enzymes associated with the proposed biosynthetic pathways, with enzymes colored in blue. The quantified metabolites detected in the present study are shown using colored boxes. The color scale was prepared based on relative GC–MS peak area percentages, with the lowest values represented in red and the highest values in dark green, and intermediate colors representing intermediate relative abundances.

In the biosynthetic pathway shown in Figure 3, acetyl-CoA serves as a key precursor and enters several pathways, including fatty acid-related metabolism. This pathway leads to the formation of metabolites such as heptanoic acid and hexanoic acid, which are further converted into derivatives including hexyl hexanoate and ethyl hexanoate through different enzymatic reactions. Among these metabolites, methyl heptanoate was detected only in *J. sabina* at 1.93%, whereas it was not detected in *J. communis*. Hexyl hexanoate was detected in *J. communis* at 0.83% but was absent in *J. sabina*. Ethyl hexanoate was also detected exclusively in *J. sabina* at 1.11% and was not observed in *J. communis* (Fig. 3).

In the conversion of hexanoic acid into other derivatives, enzymes such as lipoxygenase, alcohol dehydrogenase, and thioesterase have been reported to be associated with the formation of compounds such as hydroperoxides and 3-octanol. In this study, 3-octanol was detected only in *J. sabina* at 4.75%. Hexanoic acid was also present exclusively in *J. sabina* at 0.75%. In contrast, 1-octen-3-ol was detected only in *J. communis* at 3.23%. These differences in metabolite percentages and compound occurrence indicate species-specific variation in acetyl-CoA-associated metabolite profiles between the two species (Fig. 3).

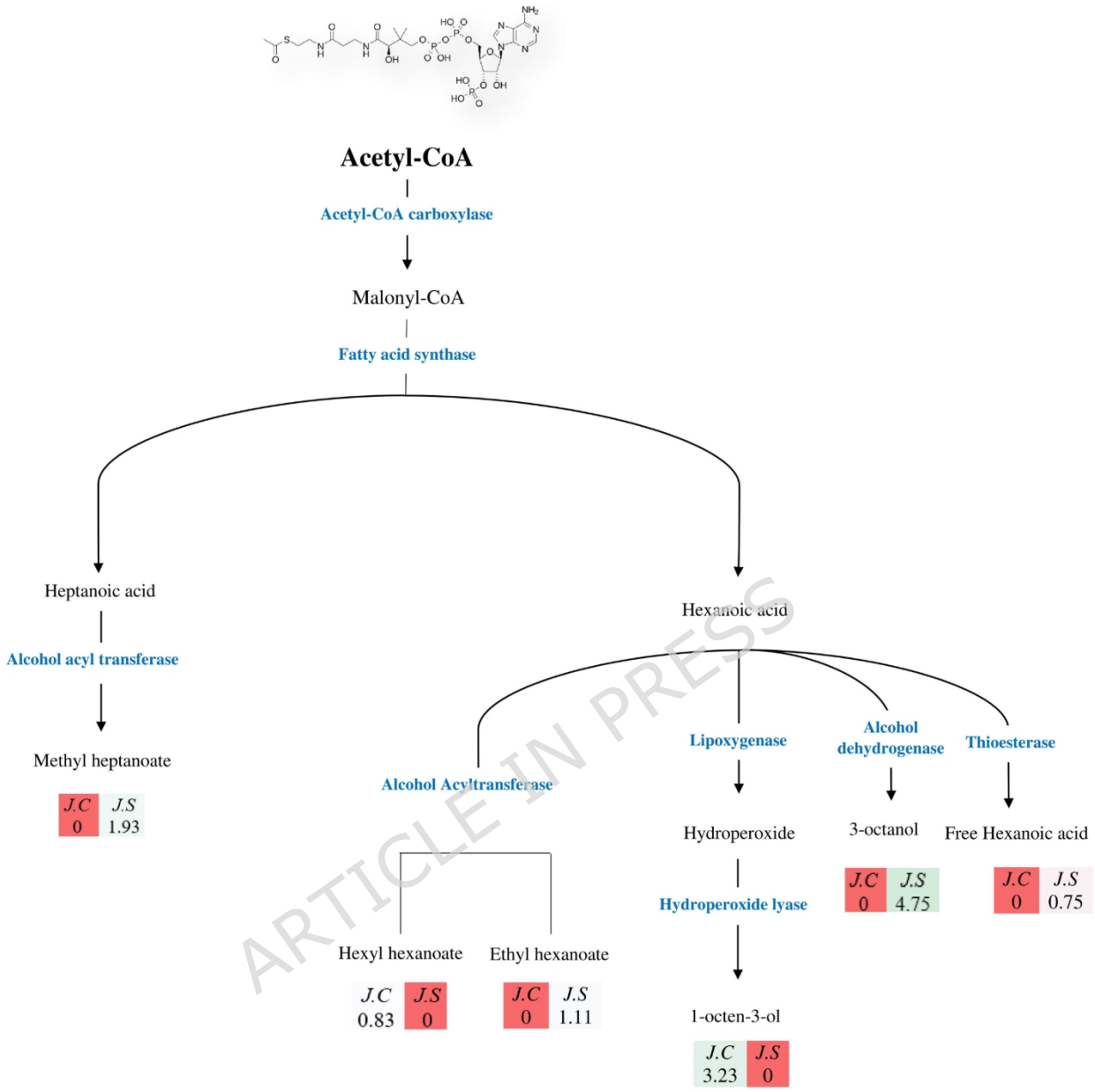

Figure 3. Schematic representation of the putative acetyl-CoA-related biosynthetic pathway in *Juniperus communis* (JC) and *Juniperus sabina* (JS). The pathway illustrates the substrates, products, and reported enzymes associated with the proposed biosynthetic pathway, with enzymes colored in blue. The quantified metabolites detected in the present study are shown using colored boxes. The color scale was prepared based on relative GC–MS peak area percentages, with the lowest values represented in red and the highest values in dark green, and intermediate colors representing intermediate relative abundances.

In this study, the biosynthetic pathway of valine and related products in two species *J. communis* and *J. sabina* were investigated. The results showed that the Ehrlich pathway branches into two compounds, Hexyl alcohol and

Isobutyl alcohol. Hexyl isovalerate, derived from Hexyl alcohol, was measured at 1.21% in *J. communis* and 0.71% in *J. sabina*. In the next pathway, Isobutyl isovalerate was measured at relative abundance of 0.67% in *J. communis* and 0.61% in *J. sabina*. Notably, Isobutyl angelate in *J. sabina* had a higher relative abundance (1.52%) compared to *J. communis* (0.8%), suggesting species-specific differences in the relative accumulation of valine-derived metabolites (Fig. 4).

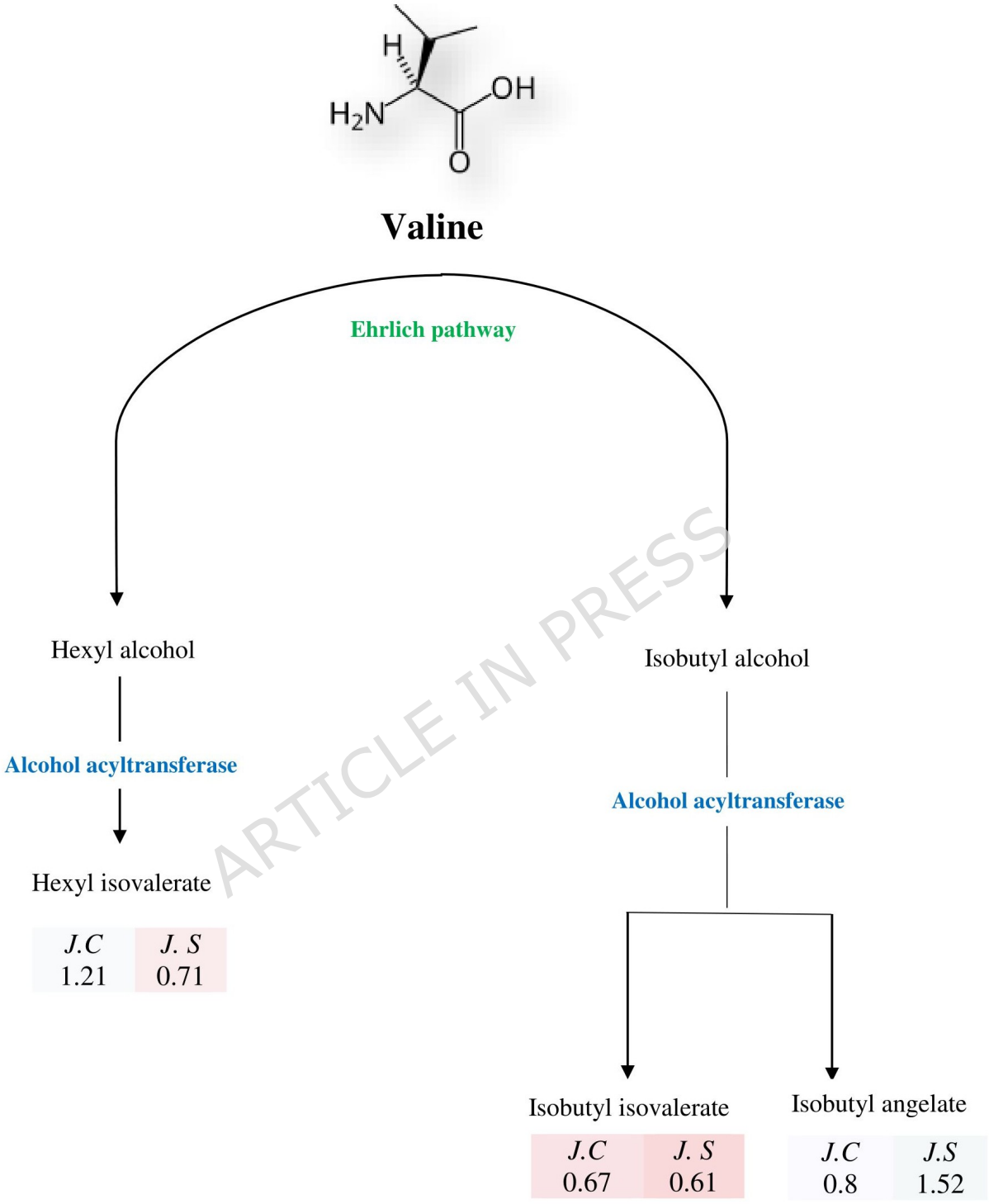

Figure 4. Schematic representation of the putative valine-related biosynthetic pathway in *Juniperus communis* (JC) and *Juniperus sabina* (JS). The pathway illustrates the substrates, products, and reported enzymes associated with the proposed biosynthetic pathway, with enzymes colored in blue. The quantified metabolites detected in the present study are shown

using colored boxes. The color scale was prepared based on relative GC–MS peak area percentages, with the lowest values represented in red and the highest values in dark green, and intermediate colors representing intermediate relative abundances.

In our experiment, the majority of the identified compounds in both species were associated with the GPP pathway, with 49 compounds present. This represents a dominant proportion of the total compounds identified, which amounted to 63 compounds, approximately 77.78% of the total. The main precursor of GPP branches into 26 distinct pathways, many of which have their own specific biosynthetic pathways. Among the most prominent compounds with high relative abundance in both species were terpinolene (*J. communis*: 6.66%; *J. sabina*: 8.04%), sabinene (*J. communis*: 4.44%; *J. sabina*: 12.78%), and *p*-cymene (*J. communis*: 2.27%; *J. sabina*: 3.34%). In *J. communis*, the compounds with the highest relative abundance included *α*-phellandrene (14.97%), *trans*-pinene (15.00%), *α*-pinene (11.28%), and *trans*-sabinene acetate (5.02%). In contrast, in *J. sabina*, camphene (10.12%), sabinene (12.78%), *δ*-terpinyl acetate (3.83%), *α*-terpinyl (6.78%), terpinene (6.78%), and linalool (3.38%) were the dominant metabolites.

Furthermore, several compounds were exclusively detected in *J. communis*, including *α*-*γ*-terpinene-7-ol (0.67%), σ-carene (2.40%), bergamal (2.27%), *β*-elemene (1.02%), *trans*-pinene (15.00%), *cis*-myrtanol (1.43%), verbenone (0.65%), *α*-fenchene (1.97%), limonene (0.79%), geranyl formate (1.93%), and myrtenyl acetate (1.08%). On the other hand, dehydroxy *cis*-linalool oxide (0.50%), camphene (10.12%), *cis*-thujone (0.50%), *cis*-pinene (2.42%), *β*-ocimene (0.94%), *β*-pinene (2.82%), *α*-cadinene (0.57%), terpinen-4-ol acetate (1.99%), *trans*-carvyl acetate (0.47%), *α*-campholenal (1.16%), bornyl acetate (2.55%), verbenol acetate (1.89%), sabinene hydrate (0.91%), sabinene hydrate acetate (0.52%), cineole (2.47%), and camphor (1.20%) were exclusively detected in *J. sabina*.

These findings indicate distinct metabolite profiles in both species, with species-specific metabolites reflecting differences in the relative abundance of compounds assigned to putative biosynthetic pathways. Based on database annotations and supporting literature, enzymes such as acetyltransferase, alcohol acetyltransferase, cytochrome P450, pinene synthase, and terpinene synthase were included as reported enzymes associated with GPP-derived pathways.

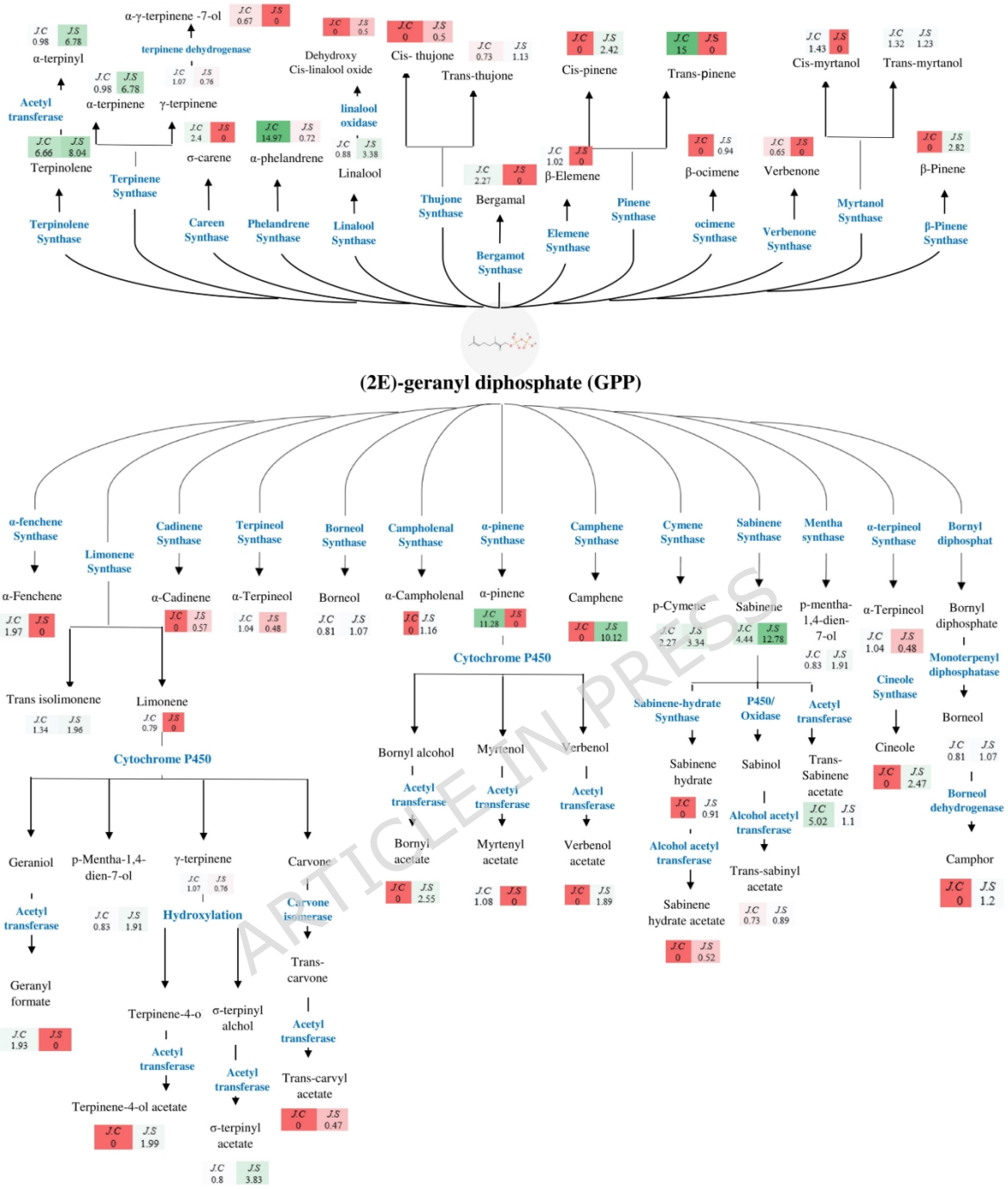

Figure 5. Schematic representation of the putative geranyl diphosphate (GPP)-related biosynthetic pathway in *Juniperus communis* (JC) and *Juniperus sabina* (JS). The pathway illustrates the substrates, products, and reported enzymes associated with the proposed biosynthetic pathway, with enzymes colored in blue. The quantified metabolites detected in the present study are shown using colored boxes. The color scale was prepared based on relative GC–MS peak area percentages, with the lowest values represented in red and the highest values in dark green, and intermediate colors representing intermediate relative abundances.

The results of our experiment showed that four products, namely *β*-Bourbonene, *α*-Copaene, *α*-Cubebene, and Artemisia Ketone, were produced from the FPP biosynthetic pathway. Except for Artemisia Ketone, which was present only in *J. sabina* (0.51%), the other three compounds were found exclusively in *J. communis*. The quantities of *β*-Bourbonene and *α*-Cubebene were similar (1.76% and 1.7% respectively), while the amount of *α*-Copaene was lower (0.71%). These results indicate significant metabolic differences between the two species, particularly in the production of various compounds derived from FPP (Fig. 6).

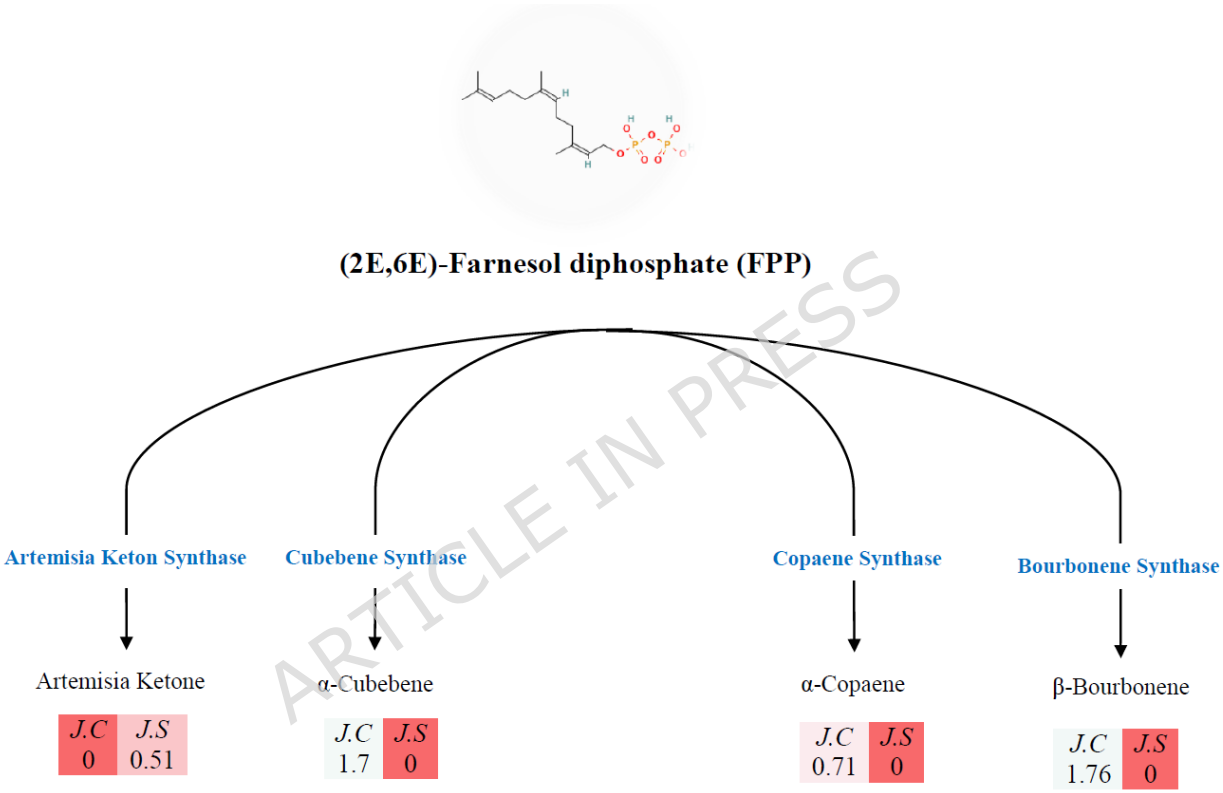

Figure 6. Schematic representation of the putative farnesyl diphosphate (FPP)-related biosynthetic pathway in *Juniperus communis* (JC) and *Juniperus sabina* (JS). The pathway illustrates the substrates, products, and reported enzymes associated with the proposed biosynthetic pathway, with enzymes colored in blue. The quantified metabolites detected in the present study are shown using colored boxes. The color scale was prepared based on relative GC–MS peak area percentages, with the lowest values represented in red and the highest values in dark green, and intermediate colors representing intermediate relative abundances.

In Figure 7, the relative abundance of metabolites associated with the shikimate/phenylalanine-related pathway was mapped for *J. communis* and *J. sabina*. Based on database annotations and supporting literature, reported enzymes such as phenylacetate synthase and phenylacetaldehyde synthase

were considered in relation to phenylalanine-derived reactions. The results showed that in *J. communis*, phenylacetic acid was mapped as a possible precursor associated with isopropyl phenylacetate (0.65%), and benzyl alcohol was mapped as a possible precursor associated with benzyl butanoate (1.41%). In contrast, these metabolites were not detected in *J. sabina* under the analytical conditions used (Fig. 7).

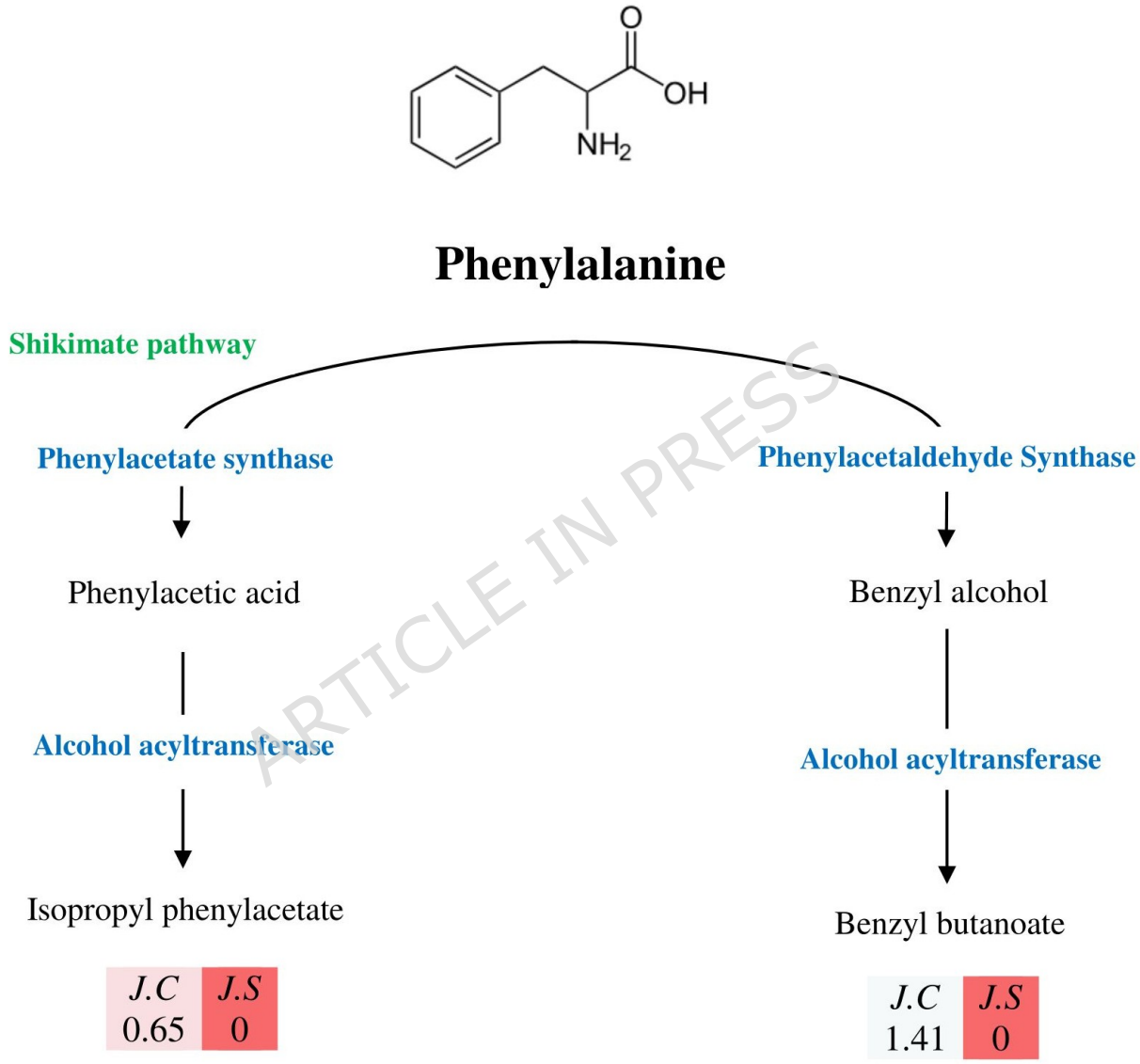

Figure 7. Schematic representation of the putative phenylalanine-related biosynthetic pathway in *Juniperus communis* (JC) and *Juniperus sabina* (JS). The pathway illustrates the substrates, products, and reported enzymes associated with the proposed biosynthetic pathway, with enzymes colored in blue. The quantified metabolites detected in the present study are shown using colored boxes. The color scale was prepared based on relative GC–

MS peak area percentages, with the lowest values represented in red and the highest values in dark green, and intermediate colors representing intermediate relative abundances.

Exploratory Multivariate Analysis of Metabolite Profiles

Principal component analysis (PCA) was used to assess the multivariate variation in GC–MS metabolite profiles of *J. communis* and *J. sabina*. The PCA biplot revealed a clear separation between the two species, primarily along Dim1, which explained 96.68% of the total variance. Dim2 explained a further 3.26% of the variance, and together the first two dimensions accounted for 99.94% of the total variation.

The *J. communis* samples were positioned on the negative side of Dim1, whereas the *J. sabina* samples were located on the positive side, indicating distinct metabolite profiles between the two species. The separation along Dim1 was associated with a broad set of metabolites. Metabolites contributing to the positive side of Dim1 included α-cadinene, ethyl hexanoate, cis-sabinene hydrate acetate, α-terpinyl acetate, β-pinene, artemisia ketone, bornyl acetate, δ-terpinyl acetate, hexanoic acid, and 3-octanol. In contrast, metabolites associated with the negative side of Dim1 included hexyl hexanoate, myrtenyl acetate, limonene, β-elemene, bergamal, β-bourbonene, and α-pinene.

The highest contributions to Dim2 were mainly related to α-terpinene-7-al, isopentyl isovalerate, trans-myrtanol, trans-sabinyl acetate, borneol, and terpinolene. However, because Dim2 explained only 3.26% of the total variance, the main species-level separation was primarily attributed to Dim1. These results indicate that the metabolic differentiation between *J. communis* and *J. sabina* is driven by coordinated differences across multiple metabolites rather than by a single compound.

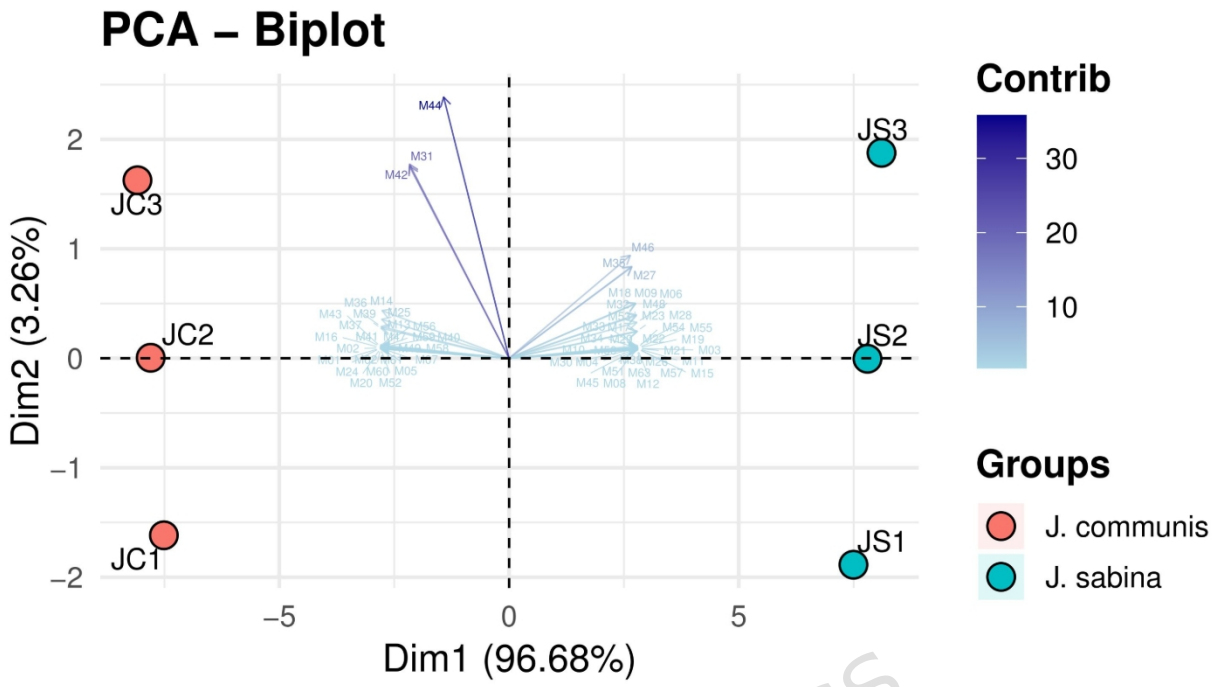

Figure 8. Principal component analysis (PCA) biplot of GC–MS metabolite profiles of *Juniperus communis* and *Juniperus sabina*. Samples are plotted according to the first two principal components, Dim1 and Dim2, which explained 96.68% and 3.26% of the total variance, respectively. The two species are separated mainly along Dim1. Metabolite vectors indicate their contribution to the PCA ordination, with darker vectors representing higher contributions. Abbreviations: JC, *Juniperus communis*; JS, *Juniperus sabina*; M01, α-Pinene; M02, α-Fenchene; M03, Camphene; M04, Hexanoic acid; M05, trans-Pinene; M06, Sabinene; M07, 1-Octen-3-ol; M08, β-Pinene; M09, trans-Isolimonene; M10, cis-Pinene; M11, 3-Octanol; M12, Ethyl hexanoate; M13, α-Phellandrene; M14, p-Mentha-1(7),8-diene; M15, Dihydroxy cis-linalool oxide; M16, δ-3-Carene; M17, α-Terpinene; M18, p-Cymene; M19, Methyl heptanoate; M20, Limonene; M21, 1,8-Cineole; M22, (Z)-β-Ocimene; M23, Isobutyl angelate; M24, Bergamal; M25, γ-Terpinene; M26, Artemisia ketone; M27, Terpinolene; M28, Linalool; M29, trans-Sabinene hydrate; M30, cis-Thujone; M31, Isopentyl isovalerate; M32, trans-Thujone; M33, α-Campholenal; M34, Camphor; M35, Borneol; M36, α-Terpineol; M37, Verbenone; M38, cis-Sabinene hydrate acetate; M39, Hexyl isovalerate; M40, cis-Myrtanol; M41, trans-Sabinene acetate; M42, trans-Myrtanol; M43, Isopropyl phenylacetate; M44, α-Terpinene-7-al; M45, Bornyl acetate; M46, trans-Sabinyl acetate; M47, γ-Terpinene-7-al; M48, Methyl acetate; M49, Geranyl formate; M50, Terpinen-4-ol acetate; M51, δ-terpinyl acetate; M52, Myrtenyl acetate; M53, p-Mentha-1,4-dien-7-ol; M54, trans-Carvyl acetate; M55, Verbenol acetate; M56, Benzyl butanoate; M57, α-terpinyl acetate; M58, α-Cubebene; M59, α-Copaene; M60, Hexyl hexanoate; M61, β-Bourbonene; M62, β-Elemene; M63, α-Cadinene.

Discussion

The present study provides a comprehensive comparative characterization of the essential oil profiles of *Juniperus communis* and *Juniperus sabina*

collected from the Salouk region of North Khorasan, Iran. The results revealed clear interspecific differences in essential oil yield, volatile composition, dominant metabolites, species-associated compounds, and multivariate chemical structure. By integrating GC–MS profiling, statistical comparison, PCA-based visualization, and database-supported biosynthetic pathway mapping, this study establishes a structured biochemical framework for understanding the chemical divergence between the two species. The overall profile highlights the importance of monoterpene-related metabolism in shaping the volatile composition of both species. These findings contribute to the phytochemical characterization of Iranian *Juniperus* species and provide candidate chemical markers that may be useful for essential oil quality assessment, chemotaxonomic comparison, and future functional studies.

Essential oil yield differed markedly between the two species, with *J. sabina* producing a higher yield than *J. communis*. This difference indicates that the two species vary not only in their qualitative volatile composition but also in their total extractable oil content under the sampling and extraction conditions used in the present study. Variation in essential oil yield is common among *Juniperus* species and can be influenced by species identity, plant organ, developmental stage, genotype, harvest season, and extraction method (Esteban et al., 2023). In the present study, both species were collected from the same general high-elevation semi-arid region and analyzed using the same extraction and GC–MS workflow. This methodological consistency strengthens the interpretation that the observed differences represent species-associated chemical patterns within the studied material. The higher essential oil yield of *J. sabina*, together with its distinctive accumulation of sabinene, camphene, oxygenated monoterpenes, and acetate derivatives, suggests that this species may represent a chemically rich source of volatile constituents for further phytochemical and applied investigations.

The GC–MS results showed that monoterpene hydrocarbons and oxygenated monoterpenes were the dominant chemical groups in both species. This finding agrees with previous studies reporting that *Juniperus* essential oils are frequently dominated by monoterpenes such as *α*-pinene, sabinene, limonene, camphene, *β*-pinene, myrcene, terpinolene, and related oxygenated derivatives (Hu et al., 2023). In *J. communis*, the most abundant constituents were *trans*-pinene, *α*-phellandrene, *α*-pinene, terpinolene, and *trans*-sabinene acetate. This composition indicates a volatile profile enriched in monoterpene hydrocarbons, which is consistent with reports on *J. communis* oils from different geographical regions where *α*-pinene, *β*-pinene,

sabinene, myrcene, and phellandrene-type compounds are commonly reported as major constituents (Raal et al., 2022; Ghanbari Moheb Seraj et al. 2022a). The relatively high abundance of *α*-phellandrene and *trans*-pinene in the present material also highlights the importance of documenting regional phytochemical patterns, because the dominance of individual compounds may vary among populations, plant organs, and environmental backgrounds.

In contrast, *J. sabina* was characterized by higher relative abundance of sabinene, camphene, terpinolene, *α*-terpinene, linalool, *δ*-terpinyl acetate, bornyl acetate, camphor, and *α*-campholenal. This profile indicates a stronger contribution of sabinene-type monoterpene skeletons and oxygenated or esterified monoterpene derivatives. Recent studies and reviews on *J. sabina* have also emphasized sabinene, *α*-pinene, camphene, terpinen-4-ol, linalool, and other oxygenated monoterpenes as important contributors to its chemical composition and biological relevance (Pan et al., 2024). The higher accumulation of oxygenated monoterpenes and monoterpene esters in *J. sabina* is particularly important because such compounds can contribute strongly to aroma quality, biological activity, and species-level chemical discrimination. Therefore, the contrast between the monoterpene-hydrocarbon-rich profile of *J. communis* and the sabinene/oxygenated-monoterpene-rich profile of *J. sabina* represents one of the central outcomes of this study.

The presence of species-associated compounds further strengthens the chemical differentiation between the two species. In *J. communis*, compounds such as *α*-pinene, *α*-fenchene, *trans*-pinene, 1-octen-3-ol, *δ*-3-carene, limonene, bergamal, verbenone, *cis*-myrtanol, geranyl formate, myrtenyl acetate, benzyl butanoate, *α*-cubebene, *α*-copaene, *β*-bourbonene, and *β*-elemene were either exclusive or more strongly represented. Conversely, *J. sabina* showed exclusive or higher accumulation of camphene, hexanoic acid, *β*-pinene, *cis*-pinene, 3-octanol, ethyl hexanoate, 1,8-cineole, *(Z)-β*-ocimene, dihydroxy *cis*-linalool oxide, artemisia ketone, *trans*-sabinene hydrate, *cis*-thujone, *α*-campholenal, camphor, bornyl acetate, terpinen-4-ol acetate, verbenol acetate, *α*-terpinyl acetate, and *α*-cadinene. These metabolite patterns provide a practical basis for distinguishing the two species and may support future authentication, quality-control, and chemotaxonomic studies.

The PCA analysis provided an additional level of evidence for species separation. While univariate analysis identified individual metabolites with significant differences, PCA summarized the overall chemical structure of the

dataset and showed that the two species formed distinct groups based on their complete metabolite profiles. The strong separation along the first principal component indicates that the differentiation between *J. communis* and *J. sabina* is not dependent on a single compound, but reflects coordinated variation across multiple volatile constituents. This is important because essential oils are complex mixtures, and their biological, aromatic, and taxonomic properties are often shaped by the combined contribution of dominant, intermediate, and minor compounds. Chemometric tools such as PCA and hierarchical clustering are widely used in essential oil studies to discriminate species, populations, plant organs, or geographical origins and to identify marker compounds (Xie and Liu, 2024; Ghanbari Moheb Seraj et al. 2021). Therefore, the inclusion of PCA strengthens the comparative metabolomics aspect of the present study and provides visual support for the species-level chemical differentiation observed in the GC–MS data.

A major biochemical feature of the present study was the predominance of GPP-associated metabolites. Among the 63 identified compounds, 49 were associated with GPP-related putative biosynthetic routes, representing approximately 77.78% of the detected volatile profile. This result is consistent with the dominance of monoterpene hydrocarbons and oxygenated monoterpenes in both species. In plant terpenoid biosynthesis, the plastidial methylerythritol phosphate pathway supplies the C5 isoprenoid precursors IPP and DMAPP, which are condensed to form geranyl diphosphate, the immediate C10 precursor of monoterpenes (Cheng et al., 2025). The high proportion of GPP-associated compounds in the present study therefore provides a coherent biochemical explanation for the monoterpene-rich character of both oils.

The distribution of GPP-derived compounds differed clearly between the two species. *J. communis* accumulated higher levels of *α*-pinene, *α*-phellandrene, *trans*-pinene, terpinolene, and *trans*-sabinene acetate, whereas *J. sabina* accumulated higher levels of sabinene, camphene, *α*-terpinene, linalool, *δ*-terpinyl acetate, bornyl acetate, camphor, and *α*-campholenal. These differences indicate that although both species are strongly characterized by monoterpene-related metabolism, the distribution of monoterpene skeletons and downstream derivatives differs substantially. Terpene synthases generate the primary hydrocarbon skeletons from prenyl diphosphate substrates, while downstream enzymes such as cytochrome P450 monooxygenases, dehydrogenases, reductases, and acyltransferases can convert these skeletons into oxygenated monoterpenes, alcohols, ketones, aldehydes, and esters (Jin et al., 2025). The higher abundance of oxygenated

and esterified monoterpenes in *J. sabina* is therefore biochemically meaningful and may explain part of the qualitative distinction between the two essential oils.

Although monoterpenes were dominant, sesquiterpene hydrocarbons also contributed to the differentiation of the two species. Compounds such as *α*-cubebene, *α*-copaene, *β*-bourbonene, and *β*-elemene were detected in *J. communis*, while *α*-cadinene was detected in *J. sabina*. Sesquiterpenes are generally associated with FPP-derived routes and can contribute to aroma complexity, defense-related chemistry, and biological activity in aromatic plants. In the present study, the relatively lower number and abundance of sesquiterpenes compared with GPP-associated monoterpenes indicate that FPP-related metabolism represented a secondary but still informative component of the volatile profile. This pattern is consistent with many *Juniperus* essential oils in which monoterpenes dominate, while sesquiterpenes contribute to finer differences among species, populations, or organs (Semerdjieva et al., 2021; Sohrabi et al. 2023).

The mapping of PEP- and shikimate/phenylalanine-related routes provides an additional framework for interpreting aromatic and phenylpropanoid-related volatiles. PEP and erythrose-4-phosphate are key entry substrates of the shikimate pathway, which leads to chorismate and then to aromatic amino acids, including phenylalanine. Phenylalanine serves as a central precursor for phenylpropanoid and benzenoid metabolism (Shende et al., 2024; Ghanbari Moheb Seraj et al. 2019). In the present study, aromatic ester and phenylpropanoid-related compounds such as isopropyl phenylacetate and benzyl butanoate were detected at lower abundance than monoterpenes. Although these compounds were not dominant constituents, their detection expands the chemical interpretation of the oils beyond terpenoid metabolism and shows that the volatile profile of these species includes minor contributions from shikimate/phenylalanine-associated routes. This is relevant because even low-abundance aromatic volatiles can contribute to aroma quality, chemical identity, and potential biological activity.

Acetyl-CoA-, fatty acid-, and amino acid-related routes also helped explain several non-terpenoid volatile compounds detected in the oils. Fatty acid-derived volatiles, including alcohols, acids, aldehydes, and esters, are common components of plant volatile blends and may arise through lipoxygenase-related reactions, alcohol dehydrogenase activity, acyltransferase reactions, and related biochemical conversions (Escobar-Bravo et al., 2023). In the present study, *J. sabina* contained methyl

heptanoate, ethyl hexanoate, hexanoic acid, and 3-octanol, whereas *J. communis* contained hexyl hexanoate and 1-octen-3-ol. These compounds demonstrate that the volatile profiles of the two species are not shaped exclusively by terpenoid metabolism, but also include contributions from fatty acid-derived and ester-forming pathways. Similarly, the occurrence of isobutyl angelate, isopentyl isovalerate, and hexyl isovalerate indicates that amino acid-related routes, including valine-associated metabolism, may contribute to the formation of branched-chain esters. Such esters can influence aroma properties and may provide additional markers for species-level differentiation.

The environmental background of the Salouk region provides useful context for interpreting the essential oil profiles. The sampled plants grew in a high-elevation, semi-arid environment with slightly alkaline sandy-loam soil, low salinity, and relatively high available nitrogen and phosphorus. Environmental factors such as water availability, light intensity, altitude, temperature, soil texture, and nutrient status can influence carbon allocation and secondary metabolite accumulation in aromatic and medicinal plants. In the present study, the shared sampling region and identical analytical workflow provide a strong basis for comparing the two species under similar environmental conditions. The soil and climatic data therefore enrich the interpretation by describing the ecological setting of the sampled material. Broader multi-location and seasonal sampling would be valuable in future studies to determine how stable these chemical differences remain across different environments and developmental stages.

From a practical perspective, the species-associated metabolite patterns identified in this study may serve as candidate chemical markers for essential oil authentication, comparative phytochemical characterization, and quality-oriented selection of plant material. Such markers may be useful in medicinal plant research, essential oil quality control, chemotaxonomic studies, and future screening programs. Recent studies have shown that essential oil composition combined with chemometric analysis can effectively discriminate Cupressaceae taxa and identify marker compounds associated with antioxidant capacity and taxonomic separation (Xie and Liu, 2024). The present study adds an Iranian dataset to this growing body of evidence and expands it by organizing the detected metabolites into a pathway-level framework.

The potential applied value of these findings is supported by previous research on *Juniperus* essential oils and their biological activities. Essential

oils from *Juniperus* species have been associated with antimicrobial, antioxidant, anti-inflammatory, insecticidal, phytotoxic, and enzyme-inhibitory properties in different experimental systems (Semerdjieva et al., 2021; Ghanbari Moheb Seraj et al. 2022b). In addition, recent reviews have highlighted the broad pharmacological and traditional relevance of *J. sabina*, including activities linked to its terpenoid-rich chemical profile (Pan et al., 2024; Ghanbari Moheb Seraj et al. 2022c). In the present study, the high relative abundance of sabinene, camphene, linalool, bornyl acetate, camphor, and other oxygenated monoterpenes in *J. sabina* makes this species a valuable candidate for future bioactivity-focused assays. Similarly, the enrichment of *J. communis* in *α*-pinene, *α*-phellandrene, *trans*-pinene, and selected sesquiterpene hydrocarbons provides a distinct chemical basis for further antimicrobial, antioxidant, or functional evaluations. These applications should be tested experimentally in future studies, but the present results provide a clear foundation for selecting target compounds and species for such work.

The database-supported pathway mapping used in this study adds value beyond simple compound listing. GC–MS studies often report essential oil constituents as isolated lists of compounds, which can make it difficult to interpret how different chemical classes are connected. By grouping the detected metabolites into PEP-, shikimate/phenylalanine-, acetyl-CoA-, valine-, GPP-, and FPP-associated routes, this study provides a more organized biochemical interpretation of the essential oil profiles. This framework helps distinguish dominant monoterpene-related metabolism from minor aromatic, fatty acid-derived, amino acid-derived, and sesquiterpene-related contributions. It also highlights candidate pathway nodes that can guide future molecular and biochemical investigations, including terpene synthase characterization, cytochrome P450-mediated oxidation, acyltransferase reactions, and isotope-assisted flux analysis.

Several points should be considered when interpreting the findings and planning future work. Compound identification was based on GC–MS library matching, retention index comparison, and literature data, which is a widely used approach in essential oil research; confirmation of selected marker compounds with authentic standards would further increase analytical precision. Quantification was based on relative peak area percentages, which effectively describes proportional differences in oil composition; future studies using absolute quantification would provide additional information on metabolite concentration per unit plant material. The present dataset included three biological replicates per species from one general

geographical region and one sampling period; broader sampling across seasons, organs, populations, and environmental gradients would help evaluate the stability of the proposed chemical markers. Finally, the pathway maps provide a strong organizational framework for the detected metabolites, and future transcriptomic, proteomic, enzymatic, and isotope-labeling studies would further deepen the functional interpretation of the proposed biochemical routes.

Overall, this study demonstrates substantial chemical differentiation between *J. communis* and *J. sabina* essential oils from the Salouk region. The two species differed in essential oil yield, dominant volatile constituents, species-associated metabolites, and multivariate chemical structure. PCA confirmed clear separation between the species, while pathway mapping showed that GPP-associated monoterpene routes formed the dominant biochemical framework of the detected volatile profiles. By combining comparative GC–MS profiling, statistical analysis, multivariate visualization, and pathway-level organization, the present study advances the phytochemical characterization of these two medicinally important *Juniperus* species and provides a useful basis for future biochemical, chemotaxonomic, quality-control, and applied research.

Conclusion

This study provides a comparative GC–MS-based characterization of volatile metabolites in *J. communis* and *J. sabina* and integrates these data with database-supported pathway mapping. The two species showed clear differences in essential oil composition. *J. communis* was characterized by higher relative abundances of *α*-pinene, *α*-phellandrene, and *trans*-pinene, whereas *J. sabina* showed higher levels of camphene, sabinene, bornyl acetate, *α*-campholenal, and camphor. These species-specific patterns indicate marked chemical differentiation between the two taxa and may serve as candidate chemical markers for comparative phytochemical characterization and essential oil quality assessment.

Pathway mapping assigned several detected metabolites to putative biosynthetic routes, including PEP-, shikimate/phenylalanine-, pyruvate-, GPP-, and FPP-related routes. The predominance of GPP-associated monoterpenes suggests that terpenoid-related metabolites play a major role in shaping the volatile profiles of both *Juniperus* species. However, these pathway assignments should be interpreted as database- and literature-supported associations, rather than direct evidence of pathway activity, metabolic flux, or enzyme-level validation.

The practical value of this study lies in identifying dominant and species-specific volatile compounds that can be prioritized for future bioactivity assays, applied phytochemical studies, and functional validation. Although the present work does not directly demonstrate pharmaceutical, agricultural, ecological, or industrial applications, it provides a structured metabolite-based basis for selecting target compounds for future antimicrobial, antioxidant, anti-inflammatory, agrochemical, and essential-oil quality studies.

Overall, this study improves the comparative chemical characterization of *J. communis* and *J. sabina* and provides a cautious pathway-mapping framework for organizing their volatile metabolites. Further transcriptomic, enzymatic, and functional studies are needed to validate the biological roles and applied potential of the candidate metabolites identified here.

Data availability statement

All data supporting the findings of this study are available within the manuscript and the supplementary files.

Funding declaration

This research received no specific grant from any funding agency in the public, commercial, or not-for-profit sectors. The authors received no financial support for the research, authorship, and/or publication of this article.

Acknowledgements

The authors would like to express their sincere appreciation to BIOCODE company for their valuable collaboration in data analysis and for providing analytical systems essential to this study. The technical support and expertise offered by this company significantly contributed to the quality and reliability of the analyses. Further information about BIOCODE company and its services is available at www.biocodeco.com.

Author Contributions Statement

M.M. conducted the experiments and was responsible for data collection. R.G.M.S. performed the data analysis and wrote the manuscript. N.T. assisted in the experiments and drew the biosynthetic pathways.

References

Ghanbari Moheb Seraj, R., Ahmadikhah, A., Esmaeilzadeh-Salestani, K., Shariati, V., Behnamian, M., Tariverdizadeh, N., ... & Dezhsetan, S. (2025a). De novo transcriptome

analysis and functional annotation of Silybum Marianum L. under drought stress with a focus on Silymarin synthesis and MAPK signaling pathways. *BMC Plant Biology*, *25*(1), 1150.

Ghanbari Moheb Seraj, R., Ahmadikhah, A., Shariati, V., & Dezhsetan, S. (2022c). Comparison of fatty acids and hydrocarbons of Milk thistle in different levels of water stress. *Journal of Plant Research (Iranian Journal of Biology)*, *35*(3), 434-449.

Ghanbari Moheb Seraj, R., Behnamian, M., Ahmadikhah, A., Shariati, V., & Dezhsetan, S. (2022b). Effect of drought stress on physiological and phytochemical traitsof Silybum marianum L. Journal of Horticultural Science. 36(1):2022, p. 135-147.

Ghanbari Moheb Seraj, R., Tohidfar, M., & Piri, H. (2019). Plant epigenetics: mechanisms and applications. Journal of Epigenetics. 1(1): 24-34.

Ghanbari Moheb Seraj, R., Tohidfar, M., Esmaeilzadeh-Salestani, K., Aliniaeifard, S., Ahmadikhah, A., Behnamian, M., ... & Sohrabi, E. (2025b). Overexpression of milk thistle SOD gene enhances drought tolerance in tobacco by improving photosynthesis and photoprotection. *Scientific Reports*.

Ghanbari Moheb Seraj, R. G. M., Mohammadi, M., Shahbazi, M., & Tohidfar, M. (2022a). Co-expression network analysis of soybean transcriptome identify hub genes under saline-alkaline and water deficit stress. *Iranian Journal of Biotechnology*, *20*(4), e3124.

Hu, R., Yu, H., Deng, J., Chen, S., Yang, R., Xie, H., ... & Yu, Y. (2025). Phosphoenolpyruvate and Related Metabolic Pathways Contribute to the Regulation of Plant Growth and Development. *International Journal of Molecular Sciences*, *26*(1), 391.

Kanehisa, M. (2019). Toward understanding the origin and evolution of cellular organisms. Protein science, 28(11), 1947-1951.

Kanehisa, M., & Goto, S. (2000). KEGG: kyoto encyclopedia of genes and genomes. Nucleic acids research, 28(1), 27-30.

Kanehisa, M., Furumichi, M., Sato, Y., Matsuura, Y., & Ishiguro-Watanabe, M. (2025). KEGG: biological systems database as a model of the real world. Nucleic acids research, 53(D1), D672-D677.

Mohammad, D. O., Vafaee, Y., Seraj, R. G. M., Mozafari, A. A., & Tahir, N. A. R. (2025). Genetic diversity of native Cucumis melo L. accessions from Iran and Iraq revealed by SCoT and ISSR markers. *Scientific Reports*.

Mohammadi, K., Mohammadi, M., Vafaee, Y., Seraj, R. G. M., & Khorshidi, J. (2025). External application of growth regulators modulates morpho-physiological traits and biochemical profiles of fennel. *Scientific Reports*, *15*(1), 41667.

Pan, L., Zhou, T., Chen, C., Xu, H., & Wang, W. (2024). Phytochemistry, Pharmacology, and Traditional Medicine Applications of Juniperus sabina L.: A Comprehensive Overview. *Molecules*, *29*(24), 5876.

Pott, D. M., Osorio, S., & Vallarino, J. G. (2019). From central to specialized metabolism: An overview of some secondary compounds derived from the primary metabolism for their role in conferring nutritional and organoleptic characteristics to fruit. *Frontiers in plant science*, *10*, 835.

Shahbazi, M., Tohidfar, M., Irani, M. A., & Seraj, R. G. M. (2022). Functional annotation and evaluation of hypothetical proteins in cyanobacterium Synechocystis sp. PCC 6803. *Biocatalysis and Agricultural Biotechnology*, *39*, 102246.

Sohrabi, E., Tohidfar, M., Ahmadikhah, A., & Seraj, R. G. M. (2023). Data-mining of barley to identify salt stress hub genes, gene expression analysis and recombinant plasmid construction. *Iranian Journal of Biotechnology*, *21*(3), e3389.

Spengler, G., Gajdács, M., Donadu, M. G., Usai, M., Marchetti, M., Ferrari, M., ... & Kovács, R. (2022). Evaluation of the antimicrobial and antivirulent potential of essential oils isolated from Juniperus oxycedrus L. ssp. macrocarpa aerial parts. *Microorganisms*, *10*(4), 758.

Tavares, W. R., & Seca, A. M. (2018). The current status of the pharmaceutical potential of Juniperus L. metabolites. *Medicines*, *5*(3), 81.

Yokoyama, R., de Oliveira, M. V., Kleven, B., & Maeda, H. A. (2021). The entry reaction of the plant shikimate pathway is subjected to highly complex metabolite-mediated regulation. *The Plant Cell*, *33*(3), 671-696.

Ouakouak H, Benchikha N, Hassani A, Ashour ML. (2019). Chemical composition and biological activity of Mentha citrata Ehrh., essential oils growing in southern Algeria. *J Food Sci Technol*. 56(12):5346-5353.

El-Kased RF, El-Kersh DM. (2022). GC-MS Profiling of Naturally Extracted Essential Oils: Antimicrobial and Beverage Preservative Actions. Life (Basel). 12;12(10):1587.

R Core Team (2025). R: A language and environment for statistical computing. R Foundation for Statistical Computing, Vienna, Austria.

Posit Team (2025). RStudio: Integrated Development Environment for R. Posit Software, PBC, Boston, MA, USA.

UniProt Consortium, T. (2018). UniProt: the universal protein knowledgebase. *Nucleic acids research*, *46*(5), 2699-2699.

Caspi, R., Billington, R., Keseler, I. M., Kothari, A., Krummenacker, M., Midford, P. E., ... & Karp, P. D. (2020). The MetaCyc database of metabolic pathways and enzymes-a 2019 update. *Nucleic acids research*, *48*(D1), D445-D453.

Wickham, H. (2016). Data analysis. In *ggplot2: elegant graphics for data analysis* (pp. 189-201). Cham: Springer international publishing.

Shende, V. V., Bauman, K. D., & Moore, B. S. (2024). The shikimate pathway: gateway to metabolic diversity. *Natural product reports*, *41*(4), 604-648.

Escobar-Bravo, R., Lin, P. A., Waterman, J. M., & Erb, M. (2023). Dynamic environmental interactions shaped by vegetative plant volatiles. *Natural product reports*, *40*(4), 840-865.

Xie, Q., & Liu, Z. (2024). Chemometrics of the composition and antioxidant capacity of essential oils obtained from six Cupressaceae taxa. *Scientific Reports*, *14*(1), 18612.

Cheng, R., Yang, S., Wang, D., Qin, F., Wang, S., & Meng, S. (2025). Advances in the biosynthesis of plant terpenoids: models, mechanisms, and applications. *Plants*, *14*(10), 1428.

Jin, W., Yang, Z., Xu, K., Liu, Q., Luo, Q., Li, L., & Xiang, X. (2025). A Comprehensive review of plant volatile terpenoids, elucidating interactions with surroundings, systematic synthesis, regulation, and targeted engineering production. *Biology*, *14*(5), 466.

Semerdjieva, I., Zheljazkov, V. D., Radoukova, T., Dincheva, I., Piperkova, N., Maneva, V., ... & Kačániová, M. (2021). Biological activity of essential oils of four juniper species and their potential as biopesticides. *Molecules*, *26*(21), 6358.

Esteban, L. S., Mediavilla, I., Xavier, V., Amaral, J. S., Pires, T. C., Calhelha, R. C., ... & Barros, L. (2023). Yield, chemical composition and bioactivity of essential oils from common Juniper (JuniPerus communis L.) from different spanish origins. *Molecules*, *28*(11), 4448.

Hu, H., Li, D., Bai, R., Zhang, W., Luo, H., & Yu, E. (2023). Chemodiversity and bioactivity of the essential oils of Juniperus and implication for taxonomy. *International Journal of Molecular Sciences*, *24*(20), 15203.

Raal, A., Komarov, R., Orav, A., Kapp, K., Grytsyk, A., & Koshovyi, O. (2022). Chemical composition of essential oil of common juniper (Juniperus communis L.) branches from Estonia. *ScienceRise: Pharmaceutical Science*, (6 (40)), 66-73.

Pan, L., Zhou, T., Chen, C., Xu, H., & Wang, W. (2024). Phytochemistry, pharmacology, and traditional medicine applications of juniperus sabina L.: A comprehensive overview. *Molecules*, *29*(24), 5876.